

ALUMINA INCLUSION BEHAVIOR DURING STEEL DEOXIDATION

Lifeng ZHANG* and Brian G. THOMAS**

* Research Associate, ** Professor
Dept of Mech. Eng., University of Illinois at Urbana-Champaign
140 Mech. Eng. Bldg., 1206 W. Green St., Urbana, IL 61801, USA
Tel: 1-217-333-6919 Fax: 1-217-244-6534
Email: zhang25@uiuc.edu; bgthomas@uiuc.edu

ABSTRACT

A computational model based on classic homogenous nucleation theory, thermodynamic analysis and numerical simulation, has been developed to study steel deoxidation by aluminum in a low carbon aluminum-killed steel ladle, which calculates the nucleation and time evolution of the alumina inclusion size distribution due to Ostwald ripening, Brownian collision and turbulent collision. Starting with rapid supersaturation with Al_2O_3 "pseudo-molecules", homogeneous nucleation is very fast, occurring mainly between $1\mu\text{s}$ and $10\mu\text{s}$. The stable inclusion nuclei are predicted to be only about 10-20 Å in diameter. The growth of inclusions smaller than $1\mu\text{m}$ in radii, is mainly controlled by diffusion of pseudo-molecules and Brownian collision, and inclusions in this range tend to be spherical. The growth of inclusions larger than $2\mu\text{m}$ in radii is mainly controlled by turbulent collisions, and inclusions in this range tend to form clusters which retain minimum feature sizes of $1\sim 2\mu\text{m}$. Inclusion size distribution can reach $0.1\sim 1\mu\text{m}$ at 6s and $0.1\sim 36\mu\text{m}$ at 100s. Stirring powder has significant effect on the inclusion size distribution, it is recommended that first stir vigorously to encourage the collision of small inclusions into large ones, followed by a "final stir" that slowly recirculates the steel to facilitate their removal into the slag while minimizing the generation of more large inclusions via collisions.

KEY WORDS: Alumina inclusions, Steel deoxidation, Nucleation, Collision, Growth, Removal, Bubble Flotation, Stirring Power

INTRODUCTION

The demand for cleaner steels increases every year. Steel cleanliness depends on the amount, morphology and size distribution of non-metallic inclusions in steel. There is a growing need to understand and predict the fundamental mechanisms of the formation and removal of inclusion particles from steel during deoxidation and refining operations in ladles and other metallurgical vessels. Inclusions arise from many sources, including deoxidation, reoxidation, slag entrapment, chemical reactions, and exogenous inclusions.^[1-8] Their origin can be identified from their composition and shape in the final product, which ranges from dendritic alumina (**Fig. 1a**^[9]), formed during deoxidation with a high oxygen content, coral structures from Ostwald ripening of dendritic inclusions (**Fig. 1b**^[10]), clusters of particles, formed by collisions of small alumina spheres (**Fig. 1c**^[11]), and large spheres of complex oxides, from liquid slag entrainment (**Fig. 1d**^[8]). Inclusion

evolution and removal is affected by diverse complex phenomena, including deoxidant quantity, composition, and morphology, vessel geometry, transport by turbulent flow, interfacial tension, diffusion coefficient, the initial oxygen content, collisions with both bubbles and other particles, reoxidation, temperature, and properties of the slag layer and vessel walls where inclusions may be removed or generated. Shortly after adding deoxidizer, particles nucleate, precipitate, and quickly grow. Inclusion growth can be controlled by diffusion of the deoxidization elements and oxygen [12-17], “Ostwald-ripening” [12, 13, 17-19], Brownian collisions [12-15, 17], turbulent collision [12-14, 18] and Stokes collision [13, 15, 17-19]. With improved computer power, better computational models of these phenomena are being developed.

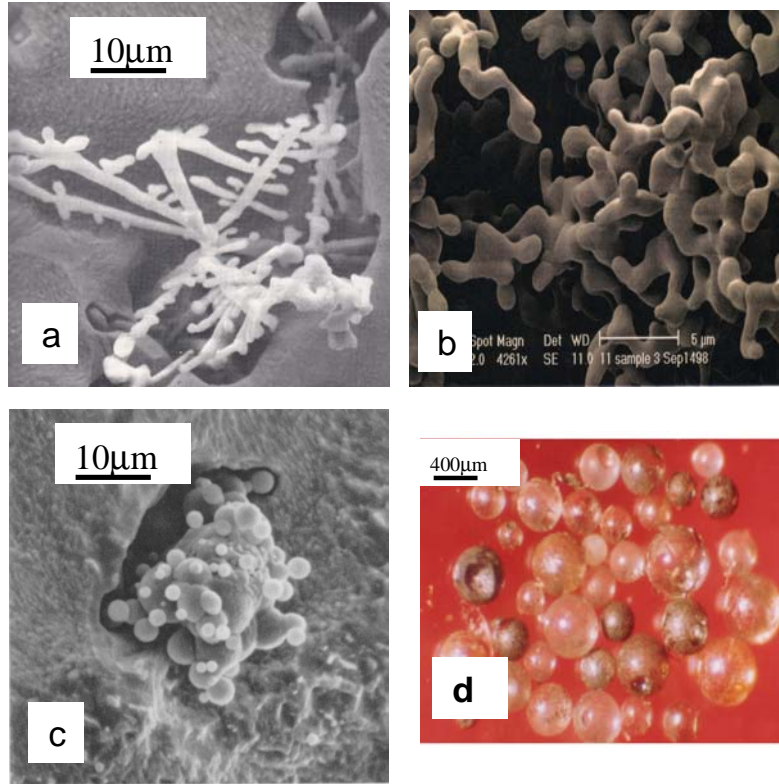


Fig. 1 Alumina inclusion morphologies: a) dendritic cluster [9], b) coral structure [10] c) alumina cluster [11], and d) slag inclusions [8]

This paper presents recent work to simulate the nucleation, growth, transport, and removal of alumina particles during steel deoxidation and discusses the implications on operations such as stirring and refining. A common characteristic of the indigenous alumina inclusions in Low Carbon Al-Killed (LCAK) steel [9-12, 20-29] is that the central globule, secondary dendrite arms, or the individual spherical inclusions in an inclusion cluster is consistently 1~4 µm (**Fig. 2**). The reason for this will be investigated in the current paper. The contribution of different growth mechanism on inclusion growth and the start and evolution of inclusion size distribution are also studied.

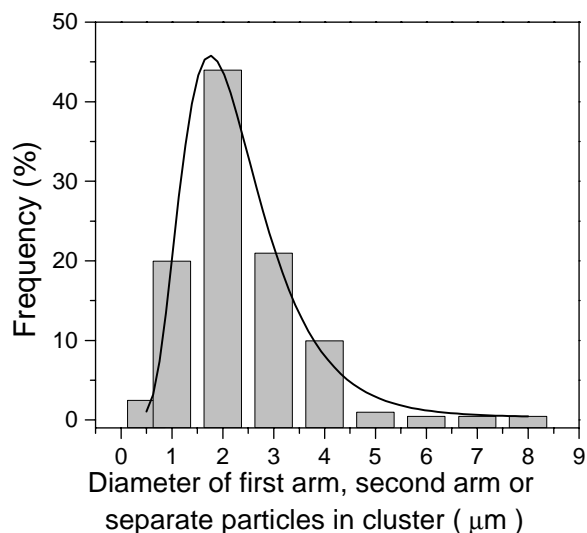


Fig. 2 The smallest size feature of inclusions as shown in Fig.1 a), b) and c).

NUCLEATION AND GROWTH MODEL FORMULATION

The current computational model simulates the nucleation and growth of alumina inclusions during steel deoxidation, starting with a solute of “pseudo-molecules” of Al_2O_3 . The assumed time-dependent concentration of pseudo-molecules evolves into a size distribution of molecular groups via diffusion and dissolution. If enough pseudo-molecules gather to form a stable nucleus, then nucleation (precipitation) occurs, meaning that the particle is stable. The stable inclusions can grow both by continued diffusion of pseudo-molecules, and by collision with other nucleated inclusions, via both Brownian and turbulent motion. The following assumptions are included in the model.

- ① The Gibbs-Thomson equation ^[30] holds for all size particles; ^[31]
- ② The basic unit of the model is the “pseudo-molecule”.
- ③ Ostwald-Ripening is considered, as both diffusion and dissolution of pseudo-molecules are calculated throughout the process.
- ④ The system is isothermal;
- ⑤ The pseudo-molecules and clusters (inclusions) are spherical;
- ⑥ The interfacial tension is independent of particle size.

If the particle size is expressed by the number of Al_2O_3 molecules in the particle, the time evolution of the pseudo-molecules / particles size distribution, N_i , is governed by the following particle number balance relations:

$2 < i < i_c$ (before nucleation)

$$\frac{dN_i}{dt} = -N_i\beta_{D,i}N_1 + \beta_{D,i-1}N_1N_{i-1} + \alpha_{i+1}A_{i+1}N_{i+1} - \alpha_iA_iN_i \quad (1)$$

$i \geq i_c$ (after formation of stable inclusion particles)

$$\begin{aligned} \frac{dN_i}{dt} = & \underbrace{-\phi N_i \sum_{j=1}^{\infty} (\beta_{B,ij} + \beta_{T,ij}) N_j + \frac{1}{2} \phi \sum_{j=1}^{i-1} (\beta_{B,j,i-j} + \beta_{T,j,i-j}) N_j N_{i-j}}_{\text{Collision of particles}} \\ & \underbrace{- N_i \beta_{D,i} N_1 + \beta_{D,i-1} N_1 N_{i-1} + \alpha_{i+1} A_{i+1} N_{i+1} - \alpha_i A_i N_i}_{\text{Diffusion of Molecules to } i \text{ and dissolution of molecules from } i} \end{aligned} \quad (2)$$

The radius of group i , r_i , is assumed to increase with the number of molecules in that group, i , by:

$$r_i = r_1 i^{1/3}, \quad (3)$$

where r_1 is the radius of a pseudo-molecule.

According to classical homogenous nucleation theory, the critical radius of nucleus r_c is

$$r_c \equiv \frac{2\sigma V_m}{RT \ln \Pi}. \quad (4)$$

If $r > r_c$, nucleation occurs, and stable particles precipitate and start to grow. According to Eq.(4), the critical size of nucleus decreases with increasing supersaturation Π and decreasing surface tension.

The supersaturation of free Al_2O_3 molecules, Π , in Eq.(4) is represented by

$$\Pi \equiv \frac{N_1}{N_{1,eq}}, \quad (5)$$

where $N_{1,eq}=2.634 \times 10^{23} \text{ m}^{-3}$ corresponds to 3ppm dissolved oxygen in steel at equilibrium. According to a mass balance, the supersaturation can be expressed by

$$\Pi = \frac{N_S}{N_{1,eq}} - \sum_{i=2}^{\infty} \frac{N_i}{N_{1,eq}} \cdot i. \quad (6)$$

where N_S is the total number of Al_2O_3 molecules including those in nucleated inclusions, which is a function of dimensionless time, represented by Eq.(7) ^[31], which defines how fast the Al_2O_3 molecules appear and disperse in the liquid steel after the deoxidizer-Al is added.

$$N_S(t) = N_{S,eq} \left[1.0 - \exp(-Kt^*) \right], \quad (7)$$

where $N_{S,eq}$ is the ultimate total number of Al_2O_3 molecules that form in the liquid steel, corresponding to the initial oxygen content before deoxidation. A rate constant K is introduced to account for the delay of the initial pseudo-molecular alumina concentration, due to reaction and diffusion of the deoxidant. ^[31]

The rate constant for pseudo-molecule diffusion, $\beta_{D,i}$, is expressed by ^[31]

$$\beta_{D,i} = 4\pi D_1 r_i. \quad (8)$$

Particle collisions are governed by the following rate constants

$$\beta_{B,ij} = \frac{2kT}{3\mu} (1/r_i + 1/r_j)(r_i + r_j), \quad (9)$$

$$\beta_{T,ij} = 1.3(r_i + r_j)^3 (\varepsilon/v)^{1/2} \quad (10)$$

where $\beta_{B,ij}$ represents Brownian collision ^[32] and $\beta_{T,ij}$ represents turbulent collision, based on Saffman's model ^[33].

Ostwald-ripening involves both growth (from diffusion governed by $\beta_{D,i}$ and dissociation, which is governed by the dissociation rate constant α_i . This dissociation rate constant is found by tracking the diffusion of pseudo-molecules, $\beta_{D,i}$. Unstable particles, ($i < i_c$) can grow or shrink only due to diffusion, while stable inclusion particles, ($i > i_c$ and $r > r_c$) evolve according to both diffusion and collision.

Eqs.(1)-(2) are solved using the Runge-Kutta method. The following material properties are chosen to model steel deoxidation at 1873K: $D_1=3.0 \times 10^{-9} \text{ m}^2/\text{s}$ (diffusion coefficient of oxygen in liquid steel) ^[34], $\rho_L=7000 \text{ kg/m}^3$, $\rho_p=2700 \text{ kg/m}^3$, $\mu_L=0.0067 \text{ kg.m}^{-1}\text{s}^{-1}$. The surface tension between Al_2O_3 particle and liquid steel is 0.5 N/m ^[35].

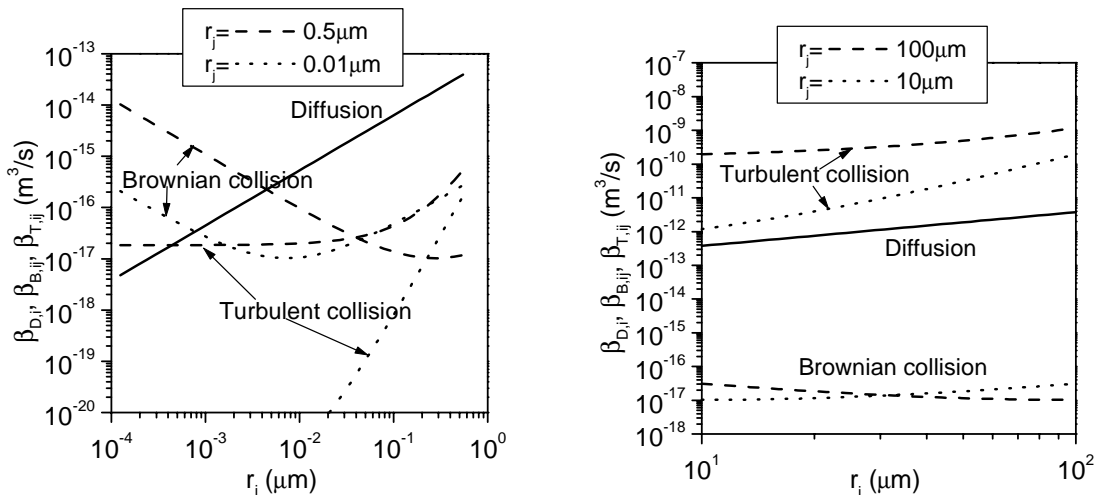


Fig. 3 Comparison of pseudo-molecule diffusion rate constant and collision rate constants

RESULTS OF NUMERICAL SIMULATION

The model was applied to aluminum deoxidation of a typical steel-oxygen system, where measurements and calculations were available. The vessel was a 50 tonne ladle of low-carbon steel refined in an ASEA-SKF furnace.^[36] The total oxygen before adding aluminum is around 300 ppm and the final free oxygen is about 3 ppm, which corresponds to a 46kg aluminum addition and gives $N_{S,eq}=100 \times N_{1,eq}$. The delay constant K was assumed to be 0.1.^[31] The ladle had 2.3m diameter and 1.7m depth, which corresponds to a turbulent energy dissipation rate in the melt of $0.01224 \text{ m}^2/\text{s}^3$ ($856.8 \text{ erg}/\text{cm}^3\text{s}$).

Control Mechanisms of Inclusion Growth at Different Inclusion Size Ranges

The following scales can be defined according to the comparison of the pseudo-molecules diffusion rate constant with the collision rate constants (**Fig. 3**):.

- Brownian scale $l_B < 1\mu\text{m}$: where the growth of inclusions with radii in this range is controlled by diffusion of pseudo-molecules and Brownian collision. The irregular thermal movement that characterizes Brownian collisions is independent of fluid flow, and is not directional. Thus the inclusions tend to grow in every direction, leading to a spherical product;
- Turbulent scale $l_T = 2 \sim l_e$, where l_e is the characteristic size of the smallest turbulence eddy, on the order of $l_e = (\nu^3/\varepsilon)^{1/4}$, and around $90\mu\text{m}$ for the current system. Inclusions with radii in this range grow by turbulent collisions, and the diffusion of pseudo-molecules is not as important, due to the low concentration of pseudo-molecules. Solid inclusions in this range tend to retain smallest features of $1 \sim 4\mu\text{m}$ in diameter as shown in Fig.2;
- Intermediate scale $l_I = l_B \sim l_T$, where the growth of inclusions in is controlled both by pseudo-molecules diffusion and by collisions (Brownian collision and turbulent collision);

Inclusion morphology is therefore summarized as follows: Fine inclusions grow spherically to 1 to 2 μm in radii due to diffusion and Brownian collision after nucleation. When there is a shortage of

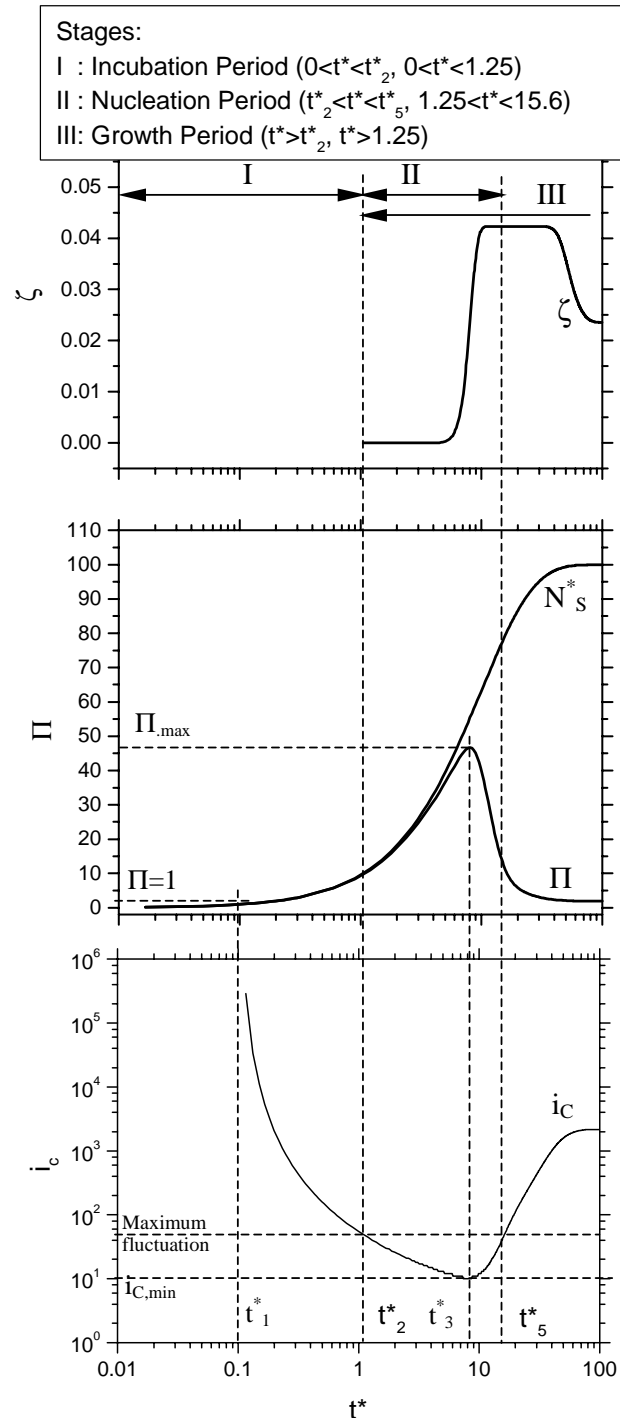


Fig. 4 Calculated ζ , Π , i_c versus time

nuclei, single particles can grow into large dendritic structures due to unstable growth into high concentrations of diffusing pseudo-molecules. Otherwise, clusters of particles will form due to turbulent collisions resulting from flowing liquid steel. With time, the surface contours of all particles becomes progressively smoother due to “Ostwald ripening”.

Incubation, Nucleation and Growth of Inclusions

Figure 4 shows the supersaturation Π , the number of particles ζ and the critical size of nucleus i_c as a function of time. After aluminum addition, the aluminum and oxygen react to form pseudo-molecules. Groups of pseudo-molecules are generated from diffusion. With the further addition and dispersion of aluminum, the concentration of pseudo-molecules continues to increase. At time $t=t_2$, the radii of some groups of pseudo-molecules become equal to r_c , thus nucleation begins. Particles precipitate and start to grow. Thus the incubation period is $0\sim t_2$. Calculation indicates that the incubation period is very short, only $0.53\mu\text{s}$. At $t=t_2$, the first particle appearing in the melt has $i_c=42$ ($r=8.3\text{ \AA}$). Thus $i=42$ is the largest group of pseudo-molecules, all of those larger than this size nucleate and become particles. After time t_2 , smaller inclusions can precipitate and grow by diffusion of pseudo-molecules, and collision with other inclusions. This starts a size distribution range. The supersaturation Π gradually increases from zero to its maximum (46.7) at time $t_3^*=8.07$ ($t_3=3.40\mu\text{s}$). This corresponds to the decrease in critical nucleus size to its smallest-sized stable nucleus ($r_c=5.15\text{ \AA}$, containing $i=10$ pseudo-molecules) at time t_3 (Eq.(4)). Groups containing less than 10 pseudo-molecules are not stable particles. Nucleation is possible only during the time period $t_2^*\sim t_5^*$ ($0.53\sim 6.58\mu\text{s}$), when the critical nucleus size is smaller than the largest sized group of pseudo-molecules (forming by random diffusion).

Figure 5 shows a histogram of inclusion size distribution at different times assuming that all inclusions with radii larger than $36\mu\text{m}$ are considered to be instantly removed to the top slag. With increasing time, this size distribution range becomes larger and larger, reaching $0.1\sim 1\mu\text{m}$ at 6s and $0.1\sim 36\mu\text{m}$ at 100s. When $t=6\text{s}$, the largest inclusion is around $2\mu\text{m}$ diameter, which agrees roughly with the industrial measurements^[37]. It takes about 100sec for the inclusions growth into several tens of microns, which agrees well with the study of Kawawa et al^[15]. Calculation indicates that after 720 seconds, the total oxygen concentration in liquid steel decreases to around 20 ppm, which agrees well with Nakanishi’s measurement.^[36]

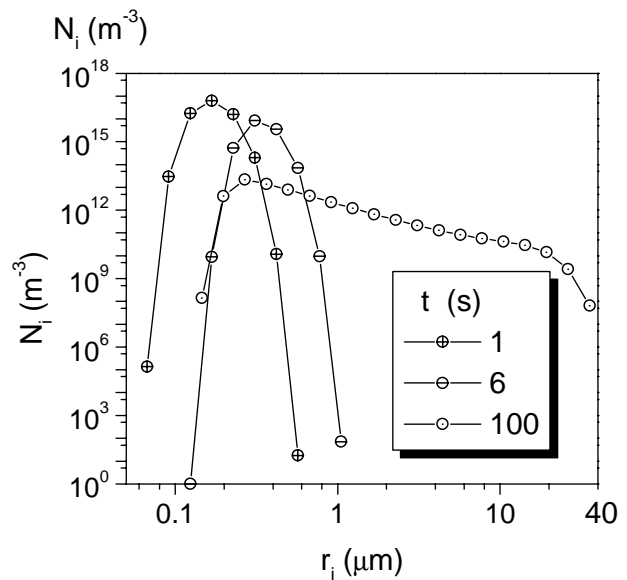


Fig. 5 Inclusion size distribution as a function of time

Effect of Stirring Power on Inclusion Evolution and removal

Stirring power is an important parameter controlling the steel refining process. Favorable metallurgical reactions require strong mixing to bring the metal and slag into contact at their interface (e.g. desulphurisation, dephosphorisation, deoxidation, and inclusion removal), whereas other detrimental phenomena favor less mixing, such as maintenance of an unbroken slag layer, and avoiding erosion of the vessel refractories. The effect of stirring power on the oxygen removal rate constant is shown in **Fig. 6**^[38, 39]. Excessively strong stirring is detrimental as the upward circulation of steel onto the slag layer may expose an “eye” region of the steel surface to reoxidation and the

lining may be seriously eroded. **Table I** gives the specific stirring powers for different refining process, based on analysis of literature data. Natural convection in the ladle and flow through the tundish produces the lowest mixing power, while vigorous stirring in NK-PERM vessels has the largest. Argon gas bubbling, DH, and steel tapping are intermediate. The SEN delivering steel into the mold has a similar stirring power to the most vigorous refining processes, although the time is very short.

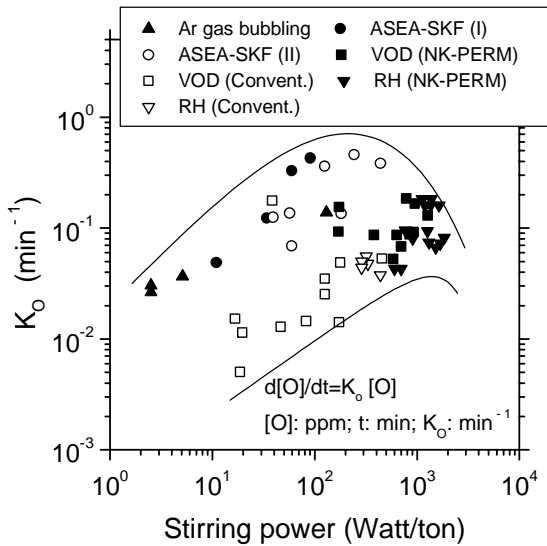


Fig. 6 Effect of stirring power on deoxidation rate constant

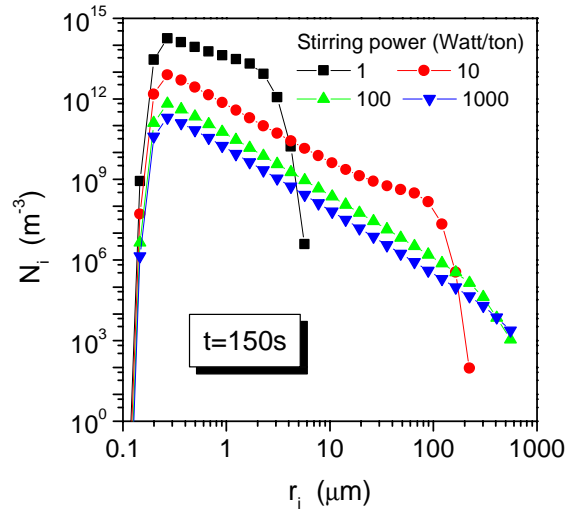


Fig. 7 Effect of stirring power on inclusion size distribution

The calculated effect of stirring power on inclusion size distribution is shown in **Fig. 7**, which indicates that increasing stirring power generates more large inclusions in the bulk. If these inclusions can be removed into the slag, this improves cleanliness. This is very bad for steel cleanliness, however, if the stirring power is high at the end of refining, when the new large inclusions have no time to be removed. Therefore, the recommended practice is to first stir vigorously, to encourage the collision of small inclusions into large ones, followed by a “final stir” that slowly recirculates the steel to facilitate their removal into the slag while minimizing the generation of more large inclusions via collisions.

Table I Stirring powers for different processes and regimes

Stirring pattern	Power (Watt/ton)
Argon gas bubbling ^[38, 40]	2-130 ^[38] , 43-214 ^[40]
Tapping steel ^[40]	17-286
DH ^[40]	72-100
ASEA-SKF ^[38, 40, 41]	7-29 ^[40] , 10-250 ^[38] , 200-600 ^[41]
PM (Pulsation Mixing) ^[40]	10
RH ^[39, 40]	86-114 ^[40] , 200-400 (conventional) ^[39] , 500-3000 (NK-PERM) ^[39]
VOD ^[39]	10-400 (conventional), 100-800 (NK-PERM)
Outlet of SEN in continuous casting mold ^[41]	470-800
Tundish inlet zone ^[41]	10-50
60 ton ladle ^[41]	1-50

CONCLUSIONS

1. A computational model based on classic homogenous nucleation theory, thermodynamic analysis and population balance equations, has been developed to study steel deoxidation by aluminum in a low carbon aluminum-killed steel ladle. The model calculates the nucleation and time evolution of the alumina inclusion size distribution due to Ostwald ripening, Brownian collision and turbulent collision.
2. For the given conditions, the nucleation is very fast, occurring mainly between 1 μ s and 10 μ s. The stable inclusion nuclei are predicted to be only about 10-20 Å in diameter (containing on the order of 10-100 pseudo-molecules of alumina). After this time, the size distribution of the stable inclusion particles grows by the diffusion / dissolution of pseudo-molecules (Ostwald-Ripening) and by collisions. The inclusion size distribution reaches 0.1~1 μ m at 6s and 0.1~36 μ m at 100s. When t=6s, the largest inclusion is around 2 μ m diameter.
3. The growth of inclusions smaller than 1 μ m, is mainly controlled by diffusion of pseudo-molecules and Brownian collision. Inclusions in this range tend to be spherical. The growth of inclusions larger than 2 μ m is mainly controlled by turbulent collisions. Inclusions in this range tend to form clusters which retain minimum feature sizes of 1~2 μ m.
4. Computations with this model of the inclusion size range in a ladle roughly agree with experimental measurements.
5. The inclusion size distribution evolves to form larger inclusions with increasing stirring power. Actual steel refining processes have a range of different stirring powers.
6. For optimal inclusion removal, it is recommended to first stir vigorously, to encourage the collision of small inclusions into large ones. This should be followed by a “final stir” that slowly recirculates the steel to facilitate their removal into the slag while minimizing the generation of more large inclusions via collisions.
7. Further studies should include the effect of deoxidant composition (Si and Al), deoxidant flow transport, interfacial tension, diffusion coefficient, the initial oxygen content, and temperature on inclusion nucleation and growth. In addition, the phenomena of bubble-related collisions, cluster morphology, reoxidation, realistic inclusion transport and collision in the turbulent flowing liquid, and removal at the top slag layer and walls on inclusion evolution also need investigation before steel deoxidation and inclusion phenomena can be fully understood.

NOMENCLATURE

A_i	The surface area of particle i , m^2
D_1	the diffusion coefficient of the pseudo-molecules in liquid, m^2s^{-1}
i, j	The particle size, namely, this particle is comprised of i pseudo-molecules or j pseudo-molecules
i_c	the critical size for nucleus
k	The Boltzmann constant, $J.K^{-1}$
N_A	The Avogadro number, mol^{-1}
N_1	The concentration of the dissolved pseudo-molecules, m^{-3}
$N_{1,eq}$	The concentration of the dissolved pseudo-molecules at equilibrium, m^{-3}
N_i	The average concentration of the particle i , m^{-3}
r	The particle radius, m
r_c	The critical radius for nucleation, m
r_i	The radii of the particle i , m
r_1	the radius of the pseudo-molecule, m
T	The absolute temperature, K
t	Time, s

t_2	Time for the beginning of nucleation, s
t_3	Time at $\Pi=\Pi_{\max}$, s
t_5	Time for the ending of nucleation period, s
t^*	The dimensionless time
α_i	The number of pseudo-molecules which dissociate per unit time from unit area of a particle of class i , $m^{-2}s^{-1}$
$\beta_{D,i}$	The diffusion rate constant of the molecules $m^3 s^{-1}$
$\beta_{B,ij}, \beta_{T,ij}$	Brownian and turbulent collision rate constant, $m^3 s^{-1}$
ε	The turbulent energy dissipation rate, m^2s^{-3}
Π	The supersaturation of the parents phase, or the dimensionless concentration of pseudo-molecules
μ	The viscosity of the liquid, $kg.m^{-1}s^{-1}$
ϕ	The inclusion oagulation coefficient ^[42]
ρ_L	The density of liquid, $kg.m^{-3}$
ρ_p	The density of particles, $kg.m^{-3}$
σ	The interfacial tension between alumina and liquid steel, $N.m^{-1}$
ζ	The total dimensionless number density of growing particles
ν	The viscosity of the liquid, m^2s^{-1}

ACKNOWLEDGEMENTS

The authors would like to thank the National Science Foundation (NSF-Grant # DMI-01-15486) and the Continuous Casting Consortium (CCC) at the University of Illinois at Urbana-Champaign (UIUC) for their support of this research. Dr. Zhang would also like to thank Prof. Wolfgang Pluschkell at Technical University of Clausthal (Germany) for ideas to start modeling nucleation.

REFERENCES

1. S. Chakraborty and W. Hill, in 77th Steelmaking Conference Proceedings, 77, ISS, Warrendale, PA, (1994), p. 389.
2. S. Chakraborty and W. Hill, in 78th Steelmaking Conference Proceedings, 78, ISS, Warrendale, PA, (1995), p. 401.
3. F.L. Kemeny, in McLean Symposium Proceedings, ISS, Warrendale, PA, (1998), p. 103.
4. B.G. Thomas and H. Bai, in Steelmaking Conf. Proc., 18, Iron and Steel Society, Warrendale, PA, (2001), p. 895.
5. M. Byrne, T.W. Fenicle and A.W. Cramb, ISS Transactions, 10, (1989), p. 51.
6. E.S. Szekeres, 4th International Conference on Clean Steel,, (Balatonszeplak, Hungary), (1992), p.
7. L. Ferro, J. Petroni, D. Dalmaso, J. Madias, C. Cicutti, Steelmaking Conference Proceeding, (Warrendale, PA), ISS, Vol. 79, (1996), p. 497.
8. L. Zhang, B.G. Thomas, X. Wang, K. Cai, in 85Steelmaking Conference Proceedings, 85, ISS, Warrandale, PA, (2002), p. 431.
9. R.A. Rege, E.S. Szekeres and W.D. Forgeng, Met. Trans. AIME, 1, (1970), p. 2652.
10. R. Rastogi and A.W. Cramb, in 2001 Steelmaking Conference Proceedings, 84, ISS, Warrendale, (Baltimore, Maryland, USA), (2001), p. 789.
11. T.B. Braun, J.F. Elliott and M.C. Flemings, Metal. Trans. B, 10B, (1979), p. 171.
12. E.T. Turkdogan, JISI, (1972), p. 21.
13. Y. Miyashita and K. Nishikawa, Trans. ISIJ, 8, (1968), p. 181.
14. S. Linder, Scand. J. Metallurgy, 3, (1974), p. 137.
15. T. Kawawa and M. Ohkubo, Trans. ISIJ, 8, (1968), p. 203.

16. E.T. Turkdogan, JISI, (1966), p. 914.
17. M. Suzuki, R. Yamaguchi, K. Murakami, M. Nakada, ISIJ Inter., 41, (2001), p. 247.
18. U. Lindborg and K. Torssell, Trans. ASME, 242, (1968), p. 94.
19. K. Nogi, Tetsu-to-Hagane, 84, (1998), p. 1.
20. K. Okohira, N. Sato and H. Mori, Trans. ISIJ, 14, (1974), p. 103.
21. M. Olette, "Institut de Recherches de La Siderurgie Francaise," Report, IRSIO, 1972.
22. K. Asano and T. Nakano, Trans. ISIJ, 12, (1972), p. 343.
23. H. Ooi, T. Sekine and G. Kasai, Trans. ISIJ, 15, (1975), p. 371.
24. N. Aritomi and K. Gunji, Trans. ISIJ, 19, (1979), p. 152.
25. N. Aritomi and K. Gunji, Trans. ISIJ, 20, (1980), p. 26.
26. Y. Miki, H. Kitaoka, T. Sakuraya, T. Fujii, ISIJ Inter., 32, (1992), p. 142.
27. W.K. Tiekink, A. Pieters and J. Hekkema, I & Smaker, 21, (1994), p. 39.
28. T. Murai, H. Matsuno, E. Sakurai, H. Kawashima, Tetsu-to-Hagane, 84, (1998), p. 13.
29. L. Zhang and S. Taniguchi, Metal. & Material Trans. B., 31B, (2000), p. 253.
30. J. Miyake and M.E. Fine, Scripta Metallurgica et Materialia, 25, (1991), p. 191.
31. L. Kampmann and M. Kahlweit, Berichte der Bunsen-Gesellschaft physikalische Chemie, 74, (1970), p. 456.
32. S. Taniguchi and A. Kikuchi, Tetsu-to-Hagane, 78, (1992), p. 527.
33. P.G. Saffman and J. S. Turner, J. Fluid Mech., 1, (1956), p. 16.
34. K. Mori and K. Suzuki, Trans. ISIJ, 12, (1972), p. 464.
35. K. Wasai and K. Mukai, Metal. & Material Trans. B., 30B, (1999), p. 1065.
36. K. Nakanishi and J. Szekely, Trans. ISIJ, 15, (1975), p. 522.
37. F. Oeters, Metallurgy of Steelmaking, Verlag Stahleisen mbH, 1994, 347.
38. K. Ogawa, in Nishiyama Memorial Seminar, 143/144, Iron and Steel Institute of Japan, (ISS, Tokyo), (1992), p. 137.
39. M. Matsuno, Y. Kikuchi, M. Komatsu, M. Arai, K. Watanabe, H. Nakashima, I & Smaker, 20, (1993), p. 35.
40. K.W. Lange, Inter. Materials Reviews, 33, (1988), p. 53.
41. L. Zhang and S. Taniguchi, International Materials Reviews, 45, (2000), p. 59.
42. T. Nakaoka, S. Taniguchi, K. Matsumoto, S.T. Johansen, ISIJ Inter., 41, (2001), p. 1103.